ACS Chemical Neuroscience

pubs.acs.org/chemneuro Research Article

Potential Metabolite Biomarkers of Multiple Sclerosis from Multiple Biofluids

Fatema Bhinderwala, Heidi E. Roth, Mary Filipi, Samantha Jack, and Robert Powers*

Cite This: *ACS Chem. Neurosci.* 2024, 15, 1110−1124 Read Online

ACCESS | Metrics & More | Article Recommendations | Supporting Information

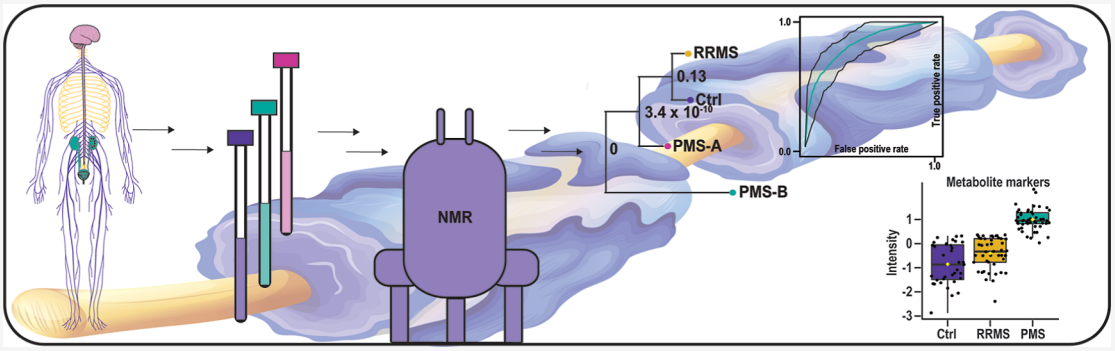

ABSTRACT: Multiple sclerosis (MS) is a chronic and progressive neurological disorder without a cure, but early intervention can slow disease progression and improve the quality of life for MS patients. Obtaining an accurate diagnosis for MS is an arduous and error-prone task that requires a combination of a detailed medical history, a comprehensive neurological exam, clinical tests such as magnetic resonance imaging, and the exclusion of other possible diseases. A simple and definitive biofluid test for MS does not exist, but is highly desirable. To address this need, we employed NMR-based metabolomics to identify potentially unique metabolite biomarkers of MS from a cohort of age and sex-matched samples of cerebrospinal fluid (CSF), serum, and urine from 206 progressive MS (PMS) patients, 46 relapsing-remitting MS (RRMS) patients, and 99 healthy volunteers without a MS diagnosis. We identified 32 metabolites in CSF that varied between the control and PMS patients. Utilizing patient-matched serum samples, we were able to further identify 31 serum metabolites that may serve as biomarkers for PMS patients. Lastly, we identified 14 urine metabolites associated with PMS. All potential biomarkers are associated with metabolic processes linked to the pathology of MS, such as demyelination and neuronal damage. Four metabolites with identical profiles across all three biofluids were discovered, which demonstrate their potential value as cross-biofluid markers of PMS. We further present a case for using metabolic profiles from PMS patients to delineate biomarkers of RRMS. Specifically, three metabolites exhibited a variation from healthy volunteers without MS through RRMS and PMS patients. The consistency of metabolite changes across multiple biofluids, combined with the reliability of a receiver operating characteristic classification, may provide a rapid diagnostic test for MS.

KEYWORDS: *metabolic biomarkers, multiple sclerosis, NMR, biofluids, cerebrospinal fluid, serum, urine*

INTRODUCTION

Multiple sclerosis (MS) is a chronic and progressive neurological disorder that affected nearly 1 million people in the United States in 2022.[1,2] MS is an autoimmune disease mediated by T and B cells[2] that damage the central nervous system (CNS) by invading the white and gray matter, leading to inflammation and ultimately the death of oligodendrocytes.[2,3] Oligodendrocytes are the cells responsible for myelin sheath formation around neurons, and the loss of these cells results in demyelination, plaque formation, and a decrease in neural transmission that leads to the many symptoms seen in MS.[3] The specific symptoms observed for a given patient will depend on lesion locations and will change with time as the disease progresses.[4] Although the cause of the immune response that leads to MS remains unclear, environmental factors such as viral and bacterial infections, smoking, vitamin deficiencies, and exposure to UV light, as well as genetic predisposition could be contributing factors.[2,3] MS presents a unique challenge for physicians since there is no known cure. Instead, a definitive diagnosis at an early stage is essential to initiate treatment and slow disease progression. Unfortunately, misdiagnosis is common due to the wide array of symptoms, the heavy reliance on neurological indicators to evaluate

Received: October 18, 2023
Revised: February 13, 2024
Accepted: February 19, 2024
Published: February 29, 2024

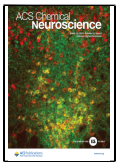

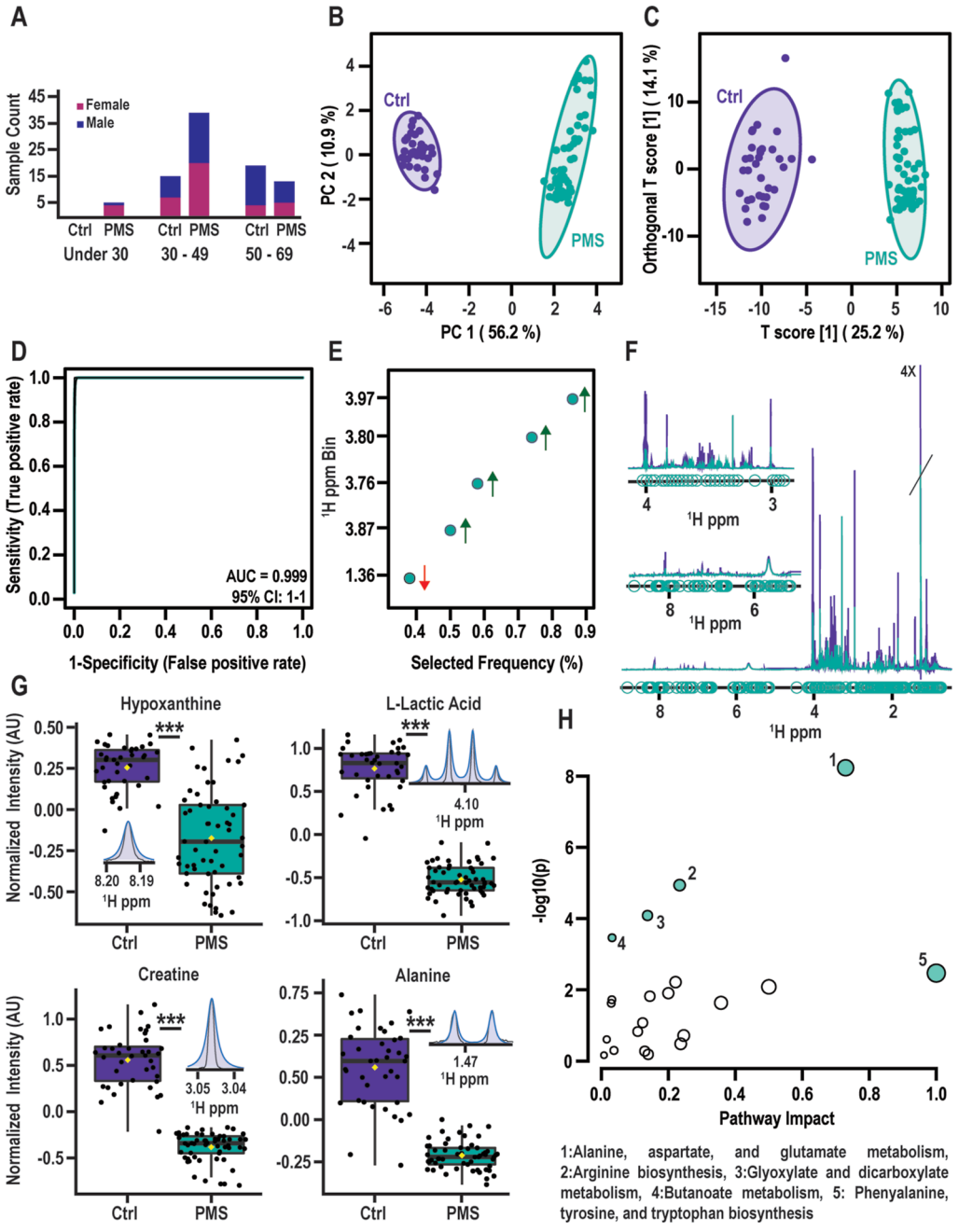

Figure 1. Metabolite biomarkers from CSF discriminate patients with progressive MS from healthy controls. (A) Age distribution of female (magenta) and male patients (blue) belonging to the Ctrl and PMS groups. All patient samples used in this comparison were pair-matched to the serum samples used in Figure 2. (B) PCA and (C) OPLS-DA score plot generated from the 1D ^{1}H NMR spectra of the CSF samples show distinct variation between progressive MS (PMS, N = 57) and the healthy control (Ctrl, N = 39) groups. PCA model yielded an R^2 of 0.671 and a Q^2 of 0.542. OPLS-DA model yielded an R^2 of 0.974, Q^2 of 0.963, and a CV-ANOVA p-value < 0.001. Permutation test used 1000 iterations. Each ellipse corresponds to the 95% confidence interval for a normal distribution of the data. (D) ROC analysis shows a five-feature multivariate model can differentiate PMS CSF samples from Ctrl with a near perfect classification accuracy (AUC = 0.999, 95% CI:1−1). (E) Frequency, contribution, and direction of spectral features used in the ROC curve in (D). Red arrows indicate a decrease in CSF and green arrows indicate an increase in CSF from PMS patients compared to Ctrl. (F) Overlays of the average 1D ^{1}H NMR spectra demonstrate the variations between Ctrl (purple) and PMS (teal). Teal points highlight bins that are significantly changing between the Ctrl and PMS spectra by Student's t-test (p-value < 0.001). Inlays show expansion of the spectral regions corresponding to 3.0−4.0 and 6.0−8.0 ppm. (G) Box and whisker plots of select CSF metabolites demonstrating relative concentration (normalized NMR peak intensities to TMSP) differences between Ctrl and PMS groups. Inserts show a representative of the expanded 1D ^{1}H NMR spectrum (red) assigned to each metabolite overlaid with the best-fit Chenomx reference spectrum (blue). Total of 244 1D ^{1}H NMR bins were used for the Chenomx analysis. Student t-test p-values followed by multiple hypotheses correction using the Benjamini-Hochberg method are indicated by *** p-value < 1×10^{-5}. (H) Pathway impact plot based on all CSF metabolites from the 1D ^{1}H NMR spectra analysis that are statistically different between Ctrl and PMS groups. Turquoise-filled circles represent pathways with p-value < 0.05 following multiple hypotheses correction using Benjamini-Hochberg method.

https://doi.org/10.1021/acschemneuro.3c00678
ACS Chem. Neurosci. 2024, 15, 1110−1124

patients according to the 2017 McDonald criteria to make a differential diagnosis (*i.e.*, a combination of patient history, magnetic resonance images, and visual evoked potentials), and the similarity of MS to numerous other neurological diseases.[5−9] Simply excluding other CNS diseases is how a diagnosis for MS is routinely achieved.[10−12] Thus, a rapid, reliable, and noninvasive diagnostic test specific for MS would benefit patients' health and well-being.[13−17]

Identifying biomarkers to aid in the diagnosis of human diseases is a well-established and successful endeavor that has the potential to decrease long-term healthcare costs.[18,19] Cerebrospinal fluid (CSF) has been the biofluid of choice for MS research because of its proximity to myelin damage and because it is expected to provide the most accurate reflection of changes in the CNS.[20−22] This has proven to be challenging, and none of the proposed CSF biomarkers have been successful to date.[23] Further, the dangers associated with spinal tap procedures to extract CSF diminish its value as a diagnostic strategy, which is why using CSF has been removed from the McDonald criteria.[24,25]

Metabolomics is a relatively new area of exploration for disease-based biomarkers,[26] where blood and urine metabolites have the potential of identifying multifluid biomarkers for a more robust and reliable disease diagnosis.[21,23,27,28] Serum is easily accessible and is a primary carrier of solutes in the body, making it a highly informative sample source.[29] Serum is also considered the most predictive phenotype due to the size of its identified metabolome.[29] Urine is a noninvasive, readily available, and less complex biofluid than CSF and serum.[30] Accordingly, urine biomarkers are considered the ideal goal for clinical applications.[30] Yet urine is highly susceptible to alterations due to variations in diet, exercise, personal habits, clinical treatments, or numerous other factors.[31] The further challenge with urine and serum metabolic biomarkers is the lack of a direct mechanistic link to MS, which may be established if the same set of metabolites observed in CSF are also observed in serum and urine.[32] There is also a growing concern regarding the accuracy and reproducibility of clinical metabolomic studies. We and others have recently identified a high rate of inconsistency across multiple clinical metabolomics, where most of the potentially identified metabolite biomarkers are simply "noise".[33−35] Instead, the detection of the same metabolite across multiple biofluids and multiple studies would be expected to increase the likelihood that a true biomarker has been discovered, which could provide the foundation for a rapid and accurate diagnostic test that will allow treatments to begin sooner while limiting the devastating effects of MS.

As a follow-up to our prior efforts to identify potential urinary metabolite biomarkers of MS,[36,37] herein, we describe the application of untargeted NMR metabolomics to identify potential biomarkers from CSF, serum, and urine to distinguish MS patients from volunteers without a MS diagnosis (*i.e.*, healthy controls). We successfully identified 32 CSF, 31 serum, and 14 urinary metabolites that significantly changed across disease states and differentiated between progressive MS (PMS), relapsing-remitting MS (RRMS), and healthy controls (Ctrl). Four metabolites, 3-hydroxybutyrate, alanine, phenylalanine, and leucine, were found to be significantly altered between PMS patients and healthy controls in all three biofluids.

RESULTS

CSF Metabolome of PMS Patients. 1D ^{1}H NMR spectra were collected for the subset of age and sex-matched CSF samples (Figure 1A), consisting of 39 healthy controls and 57 PMS patients (Table 1). The 1D ^{1}H NMR metabolomics datasets were then analyzed using multivariate statistical methods, which demonstrated a global metabolic difference between PMS patients and healthy controls. An unsupervised principal component analysis (PCA) model (Figure 1B, R^2 0.671 and Q^2 0.542) resulted in the PMS and Ctrl groups being separated into two distinct clusters in the 2D score plot, signifying unique metabolic profiles. A statistically valid (CV-ANOVA p-value < 0.001) orthogonal projection to latent structure-discriminant analysis (OPLS-DA) model (Figure 1C) further confirmed the distinct metabolomes for the PMS and Ctrl groups that also identified MS-specific metabolic changes. A receiver operating characteristic (ROC) analysis yielded a 5-feature model that classified PMS patients with a high 99.9% prediction accuracy (Figure 1D). Four of these five spectral features were increased in PMS compared to Ctrl (Figure 1E). Spectral bins that changed because of the PMS disease state were highlighted on the mean 1D ^{1}H NMR spectra calculated from the PMS and Ctrl CSF datasets (Figure 1F). A list of the assigned metabolites is provided in Supporting Information (Table S1), which includes the NMR chemical shift bins used for metabolite identification and quantification, the metabolite concentration fold changes between PMS and Ctrl, and the associated p-values indicating the statistical significance (p-value < 0.05) of the MS-induced metabolite changes. The box and whisker plots shown in Figure 1G highlight a few representative metabolite changes across all CSF samples. Additional box and whisker plots are provided in Supporting Information (Figure S1). A pathway

Table 1. Cohort Demographics[a]

class	healthy controls (Ctrl)	RRMS	PMS
sample information			
CSF samples	73[b,c] (39)	1[c] (0)	98[b,d] (57)
serum samples	44[b] (34)	52[e] (46)	196[b,d] (103)
urine samples	39[e] (26)	57[e] (0)	97[e] (46)
mean age	56.99	40.37	56.92
min/max age	19/92	35/54	21/91
female/male ratio	1:2	3:1	1:2.3

[a]The total number of samples received from the NIH NeuroBioBank or the Saunders Medical Center is listed for each type of biofluid for the three cohort groups corresponding to healthy controls, RRMS, and PMS. The numbers in parentheses are the number of samples that were used to acquire NMR spectral data for biomarker identification. The number of analyzed samples was reduced because some samples did not yield a high-quality NMR spectrum, the spectral data were outliers in an initial PCA score plot, or samples were removed to adjust for age and sex matching. Serum samples were age and sex matched to a patient's CSF (N = 57) or urine (N = 46) samples to determine the total set of samples (N = 103) analyzed by NMR for biomarker identification. [b]The biofluid samples were received from the University of Maryland Brain and Tissue Bank. [c]The biofluid samples were received from the University of Miami Brain Endowment Bank. [d]The biofluid samples were received from the Human Brain and Spinal Fluid Resource Center. [e]The biofluid samples were received from the MS Clinic within the Saunders Medical Center (Wahoo, NE, USA).

https://doi.org/10.1021/acschemneuro.3c00678
ACS Chem. Neurosci. 2024, 15, 1110−1124

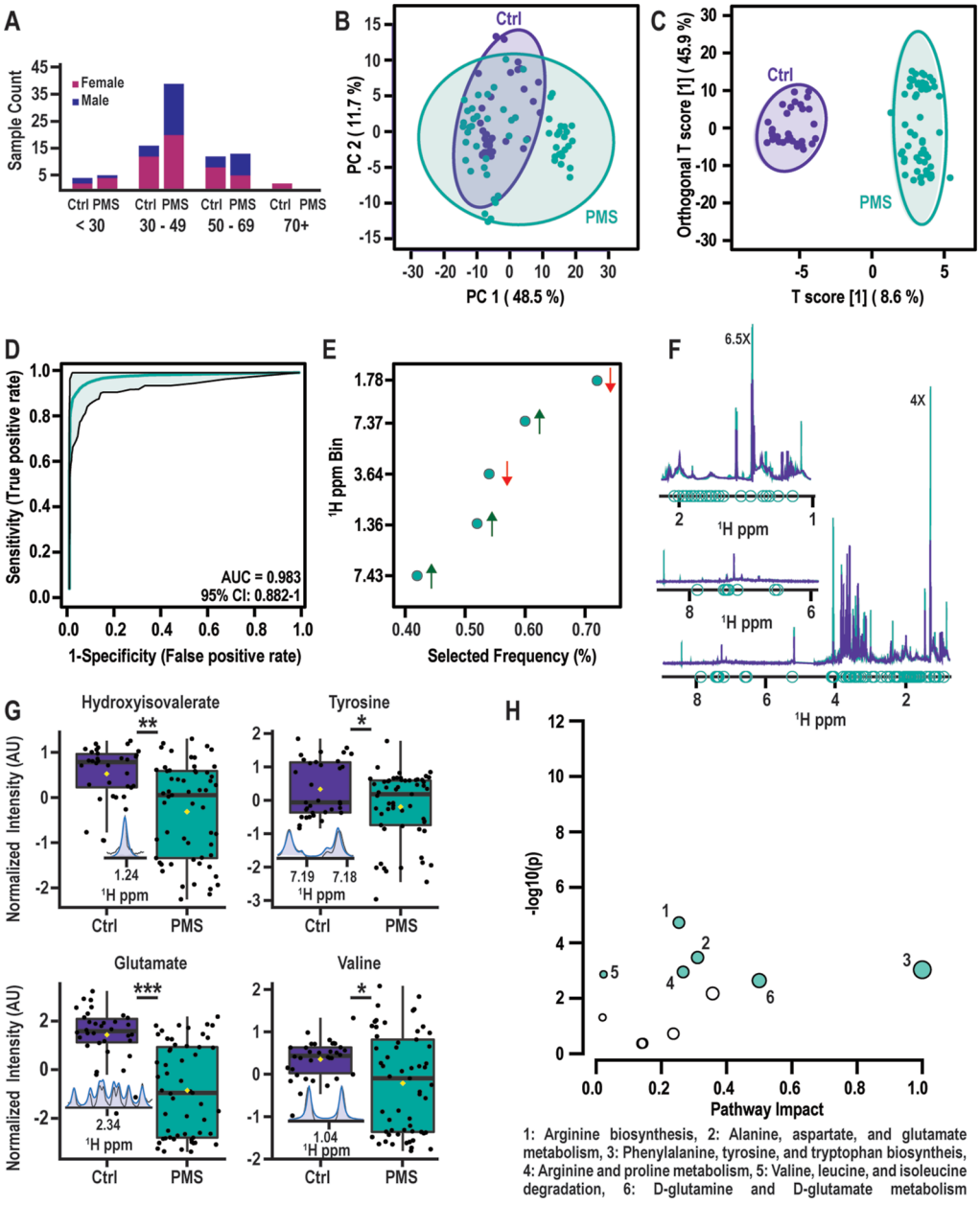

Figure 2. Metabolite biomarkers from serum discriminate patients with progressive MS from healthy controls. (A) Age distribution of female (magenta) and male patients (blue) belonging to the Ctrl and PMS groups. All patient samples used in this comparison were pair-matched to the CSF samples used in Figure 1. (B) PCA and (C) OPLS-DA score plot generated from the 1D ^{1}H NMR spectra of the serum samples show distinct variation between progressive MS (PMS, N = 57) and the healthy control (Ctrl, N = 34) groups. PCA model yielded an R^2 of 0.602 and a Q^2 of 0.568. OPLS-DA model yielded an R^2 of 0.863, Q^2 of 0.826, and a CV-ANOVA p-value < 0.001. Permutation test used 1000 iterations. Each ellipse corresponds to the 95% confidence interval for a normal distribution of the data. (D) ROC analysis shows a five-feature multivariate model can differentiate PMS serum samples from Ctrl with a high classification accuracy (AUC = 0.983, 95% CI: 0.882−1). (E) Frequency, contribution, and direction of spectral features used in the ROC curve in (D). Red arrows indicate a decrease in serum and green arrows indicate an increase in serum from PMS patients compared to Ctrl. (F) Overlays of the average 1D ^{1}H NMR spectra demonstrate the variations between Ctrl (purple) and PMS (teal). Teal points highlight bins that are significantly changing between the Ctrl and PMS spectra by Student's t-test (p-value < 0.001). Inlays show expansion of the spectral regions corresponding to 1.0−2.0 ppm and 6.0−8.0 ppm. (G) Box and whisker plots of select serum metabolites demonstrating relative concentration (normalized NMR peak intensities) differences between Ctrl and PMS groups. Inserts show a representative of the expanded 1D ^{1}H NMR spectrum (red) assigned to each metabolite overlaid with the best-fit Chenomx reference spectrum (blue). Total of 225 1D ^{1}H NMR bins were used for the Chenomx analysis. Student t-test p-values followed by multiple hypotheses correction using the Benjamini-Hochberg method are indicated by * p-value < 0.05, ** p-value < 0.001, *** p-value < 1×10^{-5}. (H) Pathway impact plot based on all serum metabolites from the 1D ^{1}H NMR spectra analysis that are statistically different between Ctrl and PMS groups. Turquoise-filled circles represent pathways with p-value < 0.05 following multiple hypotheses correction using Benjamini-Hochberg method.

impact map derived from these CSF metabolites highlights the major metabolic pathways altered by PMS (Figure 1H).

Serum Metabolome of PMS Patients. The PMS serum samples were analyzed in a manner comparable to that of the CSF samples (Figure 1). 1D ^{1}H NMR spectra were collected

https://doi.org/10.1021/acschemneuro.3c00678
ACS Chem. Neurosci. 2024, 15, 1110−1124

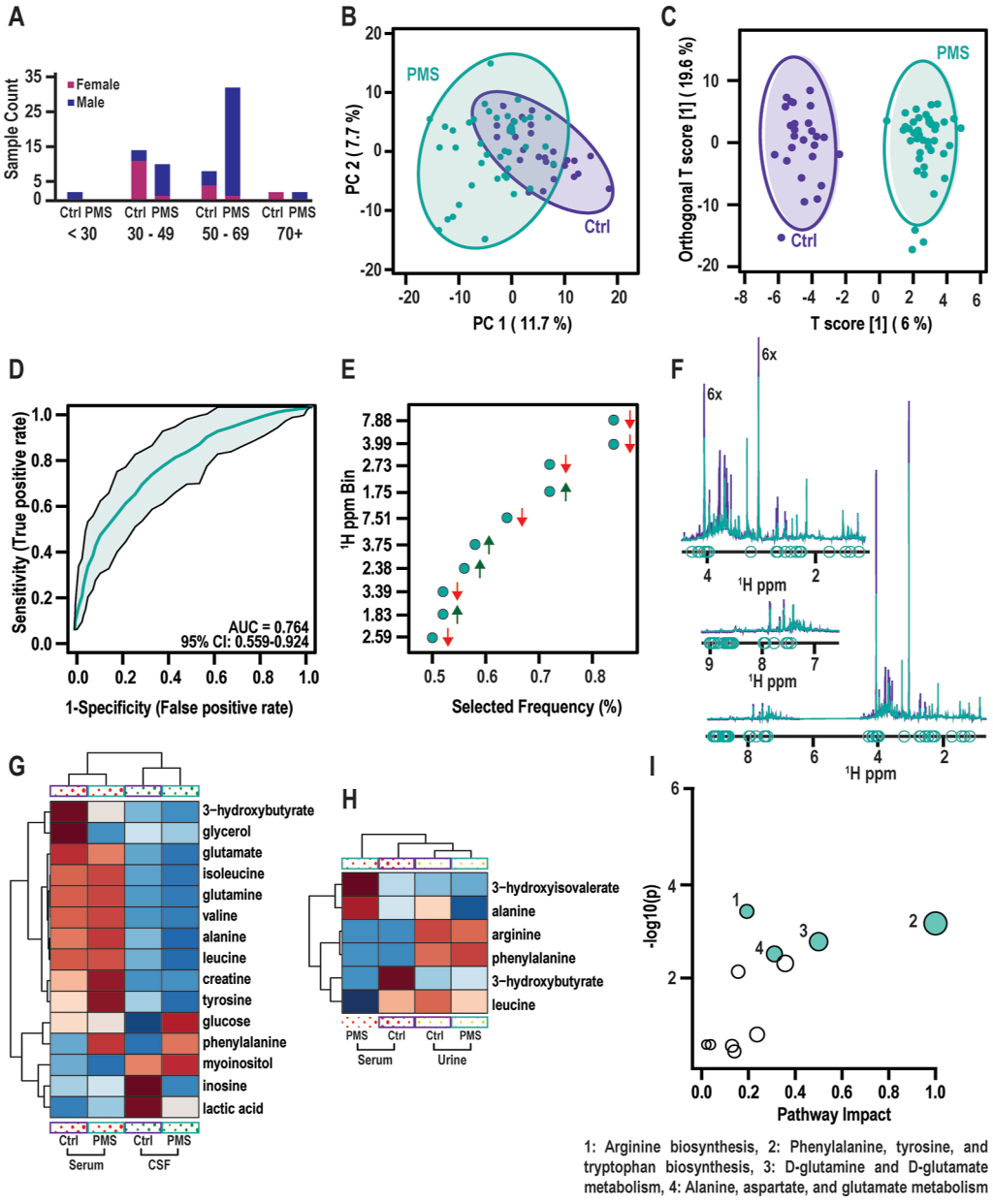

Figure 3. Metabolite biomarkers from urine discriminate patients with progressive MS from healthy controls. (A) Age distribution of female (magenta) and male patients (blue) belonging to the Ctrl and PMS groups. All patient samples used in this comparison were pair-matched to the serum samples used in Figure S2. (B) PCA and (C) OPLS-DA score plot generated from the 1D ^{1}H NMR spectra of the urine samples show distinct variation between progressive MS (PMS, $N = 46$) and the healthy control (Ctrl, $N = 26$) groups. PCA model yielded an R^2 of 0.194 and a Q^2 of 0.183. OPLS-DA model yielded an R^2 of 0.631, Q^2 of 0.480, and a CV-ANOVA p-value < 0.001. Permutation test used 1000 iterations. Each ellipse corresponds to the 95% confidence interval for a normal distribution of the data. (D) ROC analysis shows a ten-feature multivariate model can differentiate PMS urine samples from Ctrl with a nominal classification accuracy (AUC = 0.764, 95% CI: 0.559−0.924). (E) Frequency, contribution, and direction of spectral features used in the ROC curve in (D). Red arrows indicate a decrease in urine and green arrows indicate an increase in urine from PMS patients compared to Ctrl. Only the top ten of the 25 features are shown. (F) Overlays of the average 1D ^{1}H NMR spectra demonstrate the variations between Ctrl (purple) and PMS (teal). Total of 222 1D ^{1}H NMR bins were used for the Chenomx analysis. Teal points highlight bins that are significantly changing between the Ctrl and PMS spectra by Student's t-test (p-value < 0.001). Inlays show expansion of the spectral regions corresponding to 1.5−4.0 ppm and 7.0−9.0 ppm. (G) Heatmap showing mean relative metabolite concentrations and a hierarchical clustering using Euclidean distances for all commonly identified metabolites between CSF and serum samples, and their variation between Ctrl and PMS groups in the respective biofluids. (H) Heatmap showing mean relative metabolite concentrations and a hierarchical clustering using Euclidean distances for all commonly identified metabolites between serum and urine samples, and their variation between Ctrl and PMS groups in the respective biofluid. Each row in the heatmaps display the relative metabolite abundance across the four groups, where red identifies a relative metabolite accumulation and blue indicates metabolite depletion. (H) Pathway impact plot based on metabolite variations across serum and CSF samples from PMS and Ctrl groups. Turquoise-filled circles represent pathways with p-value < 0.05 following multiple hypotheses correction using Benjamini-Hochberg method.

for a subset of age and sex-matched serum samples (Table 1), consisting of 34 healthy controls and 57 PMS patients (Figure 2A). Notably, the serum samples were acquired from the same PMS patients who provided the CSF samples analyzed above.

https://doi.org/10.1021/acschemneuro.3c00678
ACS Chem. Neurosci. 2024, 15, 1110−1124

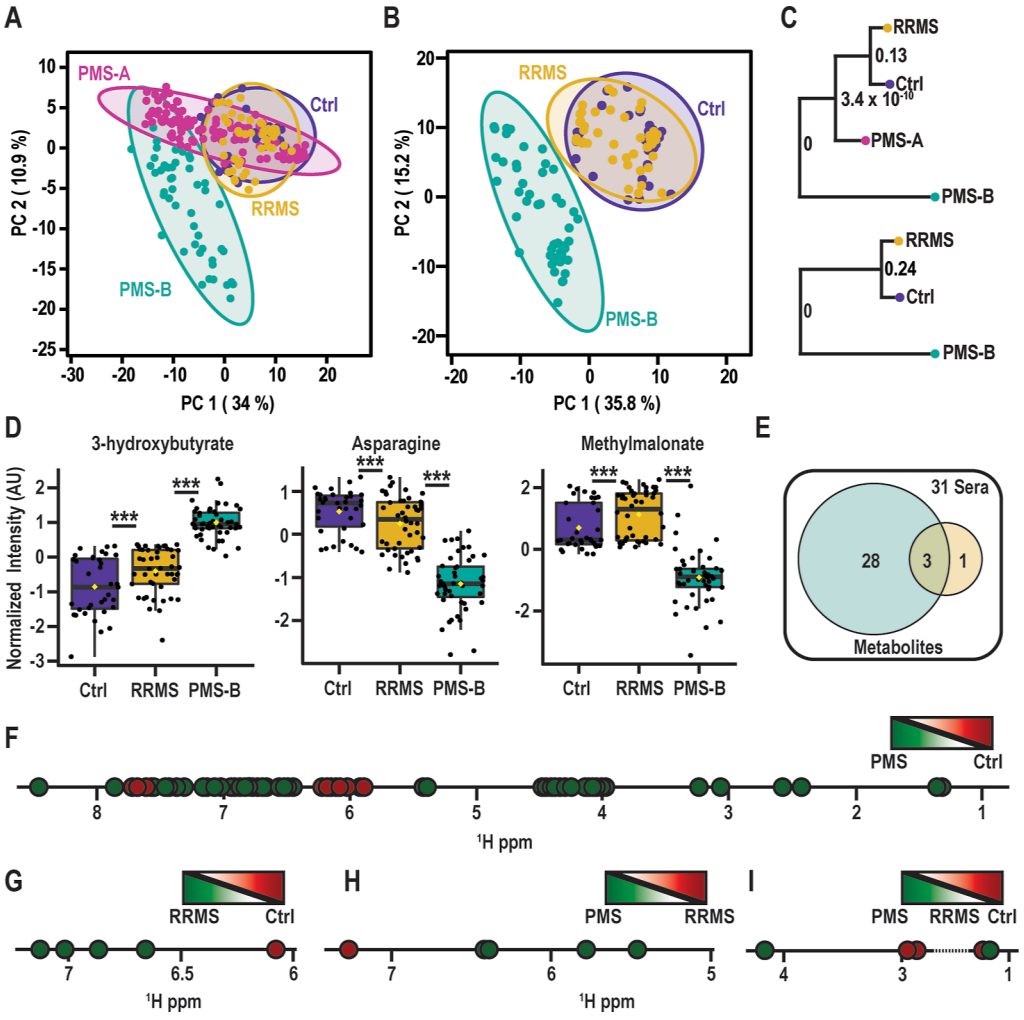

Figure 4. Metabolite biomarkers from serum discriminate PMS from RRMS. PCA score plot generated from the 1D ^{1}H NMR spectra for serum samples obtained from (A) four patient groups comprising Ctrl (purple, N = 34)), RRMS (yellow, N = 46), PMS-A (pink, N = 114), and PMS-B (teal, N = 48) (R^2 0.449 and Q^2 0.425) and (B) three patient groups comprising Ctrl (purple), RRMS (yellow), and PMS-B (teal) (R^2 0.510 and Q^2 0.473). (C) Metabolic tree diagram generated from the PCA score plot in A (top) and B (bottom). The p-value at each node is calculated from the Mahalanobis distance between each group. Coloring is identical between the PCA score plot and the tree diagram. (D) Box and whisker plots of select serum metabolites demonstrating relative concentration (normalized NMR peak intensities) differences between Ctrl (purple), RRMS (yellow), and PMS-B (teal) from the PCA model depicted in (B) Student t-test p-values followed by multiple hypotheses correction using the Benjamini-Hochberg method are indicated by *** p-value < 1×10^{-5}. (E) Venn diagram summarizing the 31 metabolites identified as altered between the Ctrl (purple), RRMS (yellow), and PMS-B (teal) serum samples in (B). Only three metabolites were altered across all three sera groups (overlap), 28 metabolites were altered in PMS-B relative to Ctrl (teal), and only one metabolite differed in RRMS relative to Ctrl (yellow). (F–I) Diagrammatic representation of a 1D ^{1}H NMR spectra showing bins that are significantly altered between the three groups (FDR adjusted p-value < 0.05). (F) Shows all spectral features significantly altered in PMS-B relative to Ctrl where a green bubble indicates an increase in intensity in PMS-B relative to Ctrl. Red bubble indicates a decrease in intensity in PMS-B relative to Ctrl. (G) 1D ^{1}H NMR spectral bins altered in RRMS relative to Ctrl. (H) 1D ^{1}H NMR spectral bins altered in PMS relative to RRMS. (I) 1D ^{1}H NMR spectral bins altered across all three groups in (B) corresponding to the three common metabolites in (D). No pair-matching restrictions were used in this comparison.

The unsupervised PCA model comparing the PMS and Ctrl serum samples yielded two partially overlapped groups in the resulting 2D score plot (Figure 2B, R^2 0.602 and Q^2 0.568). This group separation was significantly less than what was observed for the CSF samples above. Nevertheless, a statistically valid (CV-ANOVA p-value < 0.001) OPLS-DA model (Figure 2C) was produced that identified MS-specific metabolic changes in the serum from PMS patients. A ROC analysis yielded a high-quality model with a PMS prediction accuracy of 98.3% that was based on only 5 spectral features (Figure 2D). Three of these features were increased in the serum from PMS patients compared to Ctrl, while two were decreased (Figure 2E). Spectral bins that changed because of the PMS disease state are highlighted in the mean 1D ^{1}H NMR spectra calculated from the PMS and Ctrl serum datasets (Figure 2F). A list of the assigned metabolites is provided in Table S1, which includes the NMR chemical shift bins used for metabolite identification and quantification, the metabolite concentration fold changes between PMS and Ctrl, and the associated p-values indicating the statistical significance (p-value < 0.05) of the MS-induced metabolite changes. The box and whisker plots shown in Figure 2G highlight a few representative metabolite changes across all of the serum samples. Major metabolic pathways that were altered between PMS and Ctrl serum samples are shown in the pathway impact map in Figure 2H.

https://doi.org/10.1021/acschemneuro.3c00678
ACS Chem. Neurosci. 2024, 15, 1110−1124

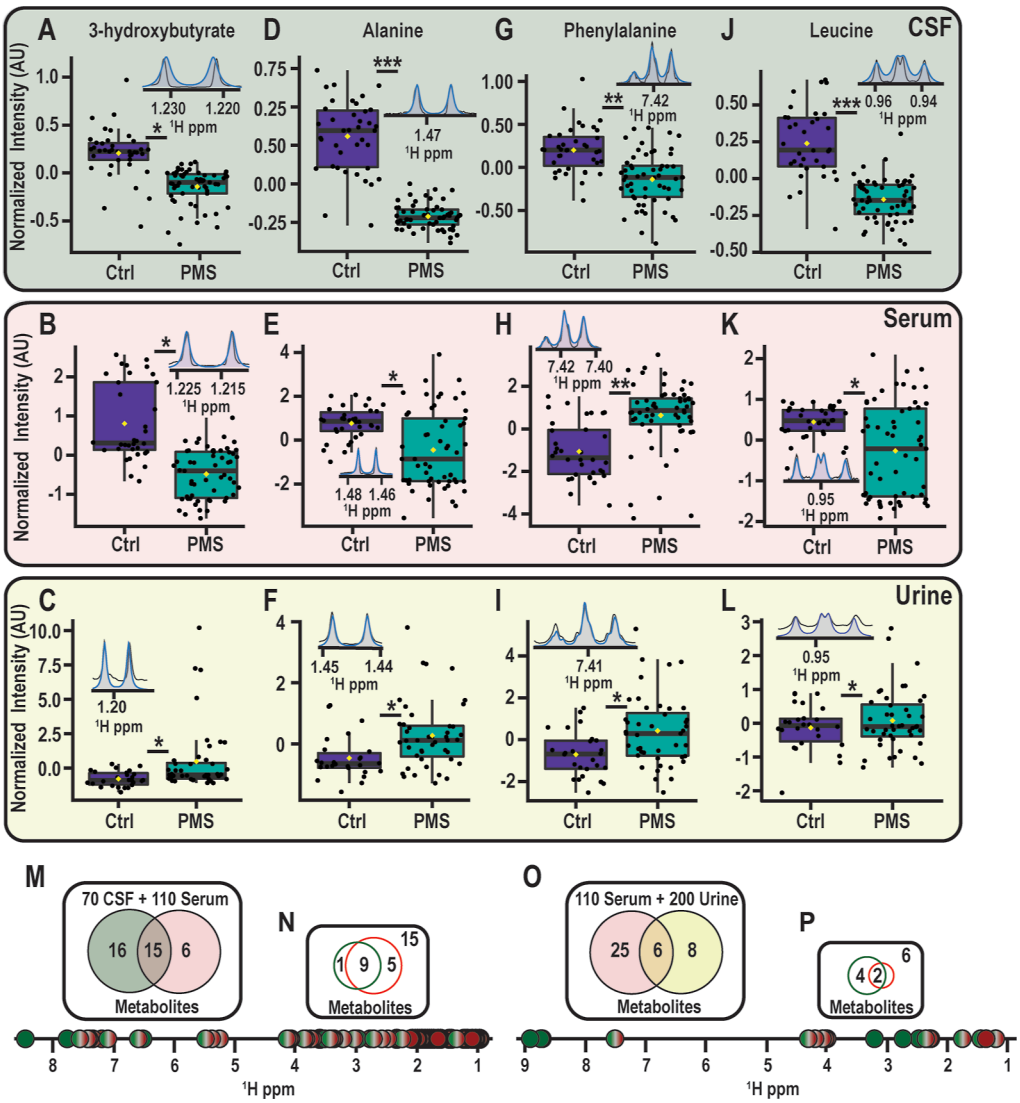

Figure 5. Metabolite biomarkers common to CSF, serum, and urine in MS. Box and whisker plots of metabolites consistently changing in CSF, serum, and urine samples of PMS patients relative to healthy controls. Number of samples used for each group and biofluid type were identical to the sample usage reported in Figures 1, 2, and 3. PMS patients relative to healthy controls in CSF: 57, 39; serum: 103, 34; and urine: 46, 26, respectively. Box plots correspond to (A−C). 3-Hydroxybutyric acid, (D−F) alanine, (G−I) phenylalanine, and (J−L) leucine. Inserts show a representative of the expanded 1D ^{1}H NMR spectrum (red) assigned to each metabolite overlaid with the best fit Chenomx reference spectrum (blue). FDR corrected *p*-values are indicated as * *p*-value < 0.05, ** *p*-value < 0.001, *** *p*-value < 1×10^{-5}. (M−P) Diagrammatic representation of 1D ^{1}H NMR spectral bins that are altered between paired CSF/serum and serum/urine samples. Green bubble indicates a decrease in PMS relative to Ctrl in both biofluids. Red bubble indicates an increase in PMS relative to Ctrl in both fluids. Multicolored bubble indicates an inconsistent change between the two biofluids (*i.e.*, one increased and one decreased). (M) Venn diagrams summarizing the total number of metabolites detected in only CSF (pink), in only serum (teal), or by both CSF and serum (overlap). (N) Venn diagram summarizing the number of overlapped metabolites (*i.e.*, 15) from (M) that are consistently increased (green, 1), decreased (red, 5), or differ (*i.e.*, one increased and one decreased) between CSF and serum samples (overlap, 9). (O) Venn diagrams summarizing the total number of metabolites detected in only serum (teal), in only urine (yellow), or by both serum and urine (overlap). (P) Venn diagram summarizing the number of overlapped metabolites (*i.e.*, 6) from (O) that are consistently increased (green, 4), decreased (red, 0), or differ (*i.e.*, one increased and one decreased) between the serum and urine samples (overlap, 2).

Serum samples acquired from PMS patients who also provided urine samples comprised a second subset of serum samples, which contained 34 healthy controls and 93 PMS patients (Figure S2A). This second subset of serum samples was analyzed in the same manner as the first subset of serum samples and yielded comparable results. The 2D score plot from the PCA model yielded a partial overlap between PMS and Ctrl samples (Figure S2B, R^2 0.463 and Q^2 0.393), but the 1D ^{1}H NMR data produced a valid (CV-ANOVA *p*-value < 0.001) OPLS-DA model (Figure S2C). A ROC analysis yielded a high-quality model with a PMS prediction accuracy of 98.2% that was based on only 5 spectral features (Figure S2D). Four of these features were decreased in the serum of PMS, while one feature was increased (Figure S2E). Spectral bins that changed because of the PMS disease state are highlighted on the mean 1D ^{1}H NMR spectra calculated from the PMS and Ctrl spectra acquired for the second subset of serum samples (Figure S2F). A list of the assigned metabolites is provided in Table S1, which includes the NMR chemical shift bins used for metabolite identification and quantification,

https://doi.org/10.1021/acschemneuro.3c00678
ACS Chem. Neurosci. 2024, 15, 1110−1124

the metabolite concentration fold changes between PMS and Ctrl, and the associated *p*-values indicating the statistical significance (*p*-value < 0.05) of the MS-induced metabolite changes. The box and whisker plots shown in Figure S2G highlight a few representative metabolite changes across the second subset of serum samples. Additional box and whisker plots are provided in Figure S3. Major metabolic pathways that were altered between the PMS and Ctrl groups using the second subset of serum samples are shown in the pathway impact map in Figure S2H.

Urine Metabolome of PMS Patients. The PMS urine samples were analyzed in a manner equivalent to that of the CSF and serum samples (Figures 1 and 2). 1D ^{1}H NMR spectra were collected for a subset of age and sex-matched urine samples (Figure 3A), consisting of 26 healthy controls and 46 PMS patients. Notably, the urine samples were acquired from the same PMS patients who provided the serum samples analyzed above. The unsupervised PCA model comparing the PMS and Ctrl urine samples showed partial group overlap in the resulting 2D score plot (Figure 3B, R^2 0.194 and Q^2 0.183), but still produced a valid (CV-ANOVA *p*-value < 0.001) OPLS-DA model (Figure 3C). The OPLS-DA model supports the presence of metabolite changes in urine samples obtained from PMS patients. The corresponding ROC analysis required significantly more spectral features than was required with either the CSF or serum samples (Figure 3D). A model based on 10 spectral features from the urine samples yielded a PMS prediction accuracy of 76.4%. The top 10 features contained 6 features that decreased in PMS and 4 features that increased in PMS (Figure 3E). Spectral bins that changed because of the PMS disease state are highlighted in the mean 1D ^{1}H NMR spectra calculated from the PMS and Ctrl urine datasets (Figure 3F). A list of the assigned metabolites is provided in Table S1, which includes the NMR chemical shift bins used for metabolite identification and quantification, the metabolite concentration fold changes between PMS and Ctrl, and the associated *p*-values indicating the statistical significance (*p*-value < 0.05) of the MS-induced metabolite changes. The box and whisker plots shown in Figure S4 highlight the metabolite changes detected in the PMS urine samples.

PMS Induces Consistent Metabolic Changes across Multiple Biofluids. The set of metabolites identified from each of the pairwise comparisons of the biofluids relative to healthy controls was then compared across the matched pairs of biofluids. Specifically, the metabolites identified from the CSF and serum samples and from the serum and urine samples obtained from the same PMS patients were compared. The combined heatmaps using the pair of CSF and serum PMS samples (Figure 3G) and the pair of serum and urine samples (Figure 3H) show distinct clustering of group averages. The heatmaps also highlight the altered metabolite concentrations in the biofluids obtained from PMS and Ctrl. Similarly, a combined impact map based on all of the metabolites identified across the three biofluids summarizes the top metabolic pathways differentially altered in PMS patients (Figure 3I).

Serum Metabolome Highlights Disease Progression from RRMS to PMS. Disease heterogeneity is a hallmark of MS, which is highlighted by the within group variance in the PCA and OPLS-DA score plots (Figure 2B,C). Furthermore, a PCA model initially generated from the complete set of 196 serum samples from PMS patients produced two distinct groupings in the score plot. These PMS groups were identified as PMS-A (N = 114) and PMS-B (N = 48) and then compared to the Ctrl (N = 34) and RRMS (N = 46) groups in a PCA model (Figure 4A, R^2 0.449 and Q^2 0.425). Please note that any replicate that fell outside the 95% confidence interval for the entire PCA model was excluded from the analysis. Accordingly, 6 RRMS, 10 healthy controls, and 34 PMS serum samples were excluded from the final PCA models, as depicted in Figure 4A,B. The resulting PCA score plot indicated a clear overlap of the Ctrl and RRMS groups, and a partial overlap with PMS-A. The removal of the PMS-A group yielded a PCA score plot with a distinct separation of the PMS-B group from the two remaining groups (Figure 4B, R^2 0.510 and Q^2 0.473). Tree diagrams (Figure 4C) derived from score plots in Figure 4A (top) and Figure 4B (bottom) show significant phenotypic variations between PMS-A and PMS-B. The box plots for 3-hydroxybutyrate, asparagine, and methylmalonate highlight the significant metabolic changes that occurred across the Ctrl, RRMS, and PMS-B groups (Figure 4D). These were the only serum metabolites identified as significantly changing across the three groups. The resulting Venn diagram in Figure 4E summarizes the metabolite comparison among the Ctrl, RRMS, and PMS groups. Overall, 28 metabolites were significantly different between the PMS and Ctrl groups, and 2 metabolites differentiated RRMS from Ctrl. Line plots illustrate the spectral differences across the serum samples from the Ctrl, RRMS, and PMS groups (Figure 4F−I). Spectral features significantly changing (*p*-value < 0.05) between PMS and Ctrl are extensive, with variations across the entire 1D ^{1}H NMR spectrum (Figure 4F). Conversely, a minimal number of spectral features were uniquely varied between RRMS and Ctrl (Figure 4G), and between PMS and RRMS (Figure 4H). The spectral features associated with the three metabolites that changed across PMS, RRMS, and Ctrl showed a narrow distribution (Figure 4I).

PMS Induces a Consistent Metabolic Profile across Three Biofluids. Our in-depth analyses of the CSF, serum, and urine biofluids led to the discovery of four unique metabolites that significantly changed between the PMS and Ctrl groups. These metabolites are 3-hydroxybutyrate (Figure 5A−C), alanine (Figure 5D−F), phenylalanine (Figure 5G−I), and leucine (Figure 5J−L). The box plots summarize the magnitude and direction of these metabolite changes in CSF (top, green), serum (middle, red), and urine (bottom, yellow). Venn diagrams with corresponding line plots (Figure 5M−P) further summarized the commonalities of metabolites between paired biofluids (*i.e.*, CSF/serum and serum/urine). The total number of metabolites identified from the 1D ^{1}H NMR datasets is shown at the top of each Venn diagram. Specifically, the paired CSF and serum samples shared 15 metabolites, where 16 metabolites were unique to CSF and 6 metabolites were unique to serum (Figure 5M). The Venn diagram in Figure 5N summarizes the number of these 15 shared metabolites that were consistently increased (green, 1) or decreased (red, 5) in both the CSF and serum samples from PMS patients. It also indicates that 9 metabolites exhibited an inconsistent change between these two biofluids. While the 9 metabolites were statistically different in CSF and serum relative to Ctrl, the direction of the observed change was also different. For example, a metabolite that was increased in CSF relative to Ctrl was decreased in serum or *vice versa*. Similarly, the paired serum and urine samples shared 6 metabolites, where 25 metabolites were unique to serum and 8 metabolites

https://doi.org/10.1021/acschemneuro.3c00678
ACS Chem. Neurosci. 2024, 15, 1110−1124

were unique to urine (Figure 5O). The Venn diagram in Figure 5P summarizes the number of these 6 shared metabolites that were consistently increased (green, 4) or decreased (red, 0) in both the serum and urine samples from PMS patients. It also indicates that 2 metabolites exhibited an inconsistent change between these two biofluids.

DISCUSSION

CSF Metabolome Links Diverse Metabolic Pathways to MS. The 32 metabolites altered in the CSF of PMS patients relative to healthy controls (Table S1) were directly associated with a range of cellular or biological processes that contribute to the pathology of MS. The 32 CSF metabolites were primarily amino acids and metabolites related to glycolysis and TCA, which included succinate, acetate, lactate, and glycerol, which all decreased in PMS. Conversely, glucose, formate, and citrate were increased in PMS CSF. A decrease in lactate and an increase in glucose suggested an overall decrease in glycolytic activity, and, consequently, a decrease in the synthesis of the metabolic precursors necessary for protein and lipid biosynthesis that is vital for myelin production.[38] A decrease in TCA metabolites has been previously implicated in various encephalopathies.[39] Proper brain and neuronal function is highly dependent on the availability and efficient utilization of glucose, where dysfunctional glycolysis can quickly lead to cognitive impairment and brain damage.[40−42]

Alanine, which was decreased in PMS CSF, can be used to generate energy *via* the glucose−alanine shuttle when glucose levels are low or as a potential alternative to dysregulated glycolysis, as we observed in the CSF of PMS patients. Notably, alanine can also be synthesized from branched-chain amino acids (BCAAs). BCAA isoleucine, leucine, and valine were all decreased in the CSF from PMS patients, which is consistent with the prior observation that BCAAs were decreased in the CSF from MS patients.[43,44] BCAAs have been attributed to muscle tremors, a decrease in appetite, lethargy, and neurological defects.[45] Lower levels of BCAAs may also impair regulatory T cells, which may result in increased inflammatory T cell activity.[46] Ketone 3-hydroxybutyrate (3-HB) was also decreased in the CSF of PMS patients. 3-HB is a partial degradation product of BCAAs and can be used as a source of energy by the brain under glucose deprivation or ketosis.[47] Again, this is consistent with the overall decrease in glycolytic activity that was observed in the PMS CSF. 3-HB is also known to decrease lipolysis, inflammation, and reactive oxygen species (ROS).[47]

Glycine, aspartate, and *N*-acetyl-L-aspartate (NAA) were found to decrease in the CSF from PMS patients. Glycine serves as an inhibitory neurotransmitter in the CNS, while 3-aminoisobutanoate, which was decreased in PMS CSF, serves as a partial agonist of the glycine receptor.[48] Conversely, aspartate is a major excitatory neurotransmitter and NAA is a precursor to the neurotransmitter *N*-acetylaspartylglutamate (NAAG).[49] Glutamine and glutamate were also found to be decreased in PMS CSF. Glutamate is the most abundant excitatory neurotransmitter in the CNS. Neuronal glutamine uptake is vital for conversion to glutamate, which is a vital precursor of the inhibitory neurotransmitter gamma-aminobutyric acid (GABA).[50] Similar to glutamate and glutamine, GABA was found to decrease in PMS CSF. As vital neurotransmitters, glutamate and GABA are targets in the development of neuroprotective therapies.[50] Glutamine is also vital to protect against neurotoxicity due to an increase in ROS.[51] Thus, a decrease in both 3-HB and glutamine levels may lead to a higher level of ROS-induced neuronal damage in MS patients. Both phenylalanine and tyrosine were found to decrease in PMS. Both serve as precursors for the neurotransmitter dopamine.[52] These metabolic changes are consistent with neurotransmitters playing an important role in the pathogenesis of MS.

NAA is also important to myelin synthesis, where its decrease in CSF may suggest a disruption of myelin repair. Myoinositol was likely dysregulated in PMS, which is an important component of myelin and has been proposed to be related to the development of peripheral neuropathy in diabetic patients.[53] Again, the overall decrease in glycolytic activity and the reduction in the metabolic precursors vital to myelin production would be consistent with a disruption in myelin repair.[38] The observation that *β*-*N*-acetylglucosamine was increased in PMS CSF provides further support for a dysfunctional myelin repair process. *β*-*N*-acetylglucosamine has been shown to be a critical regulator of myelination and myelination repair in mice.[54] Taken together, these metabolic changes in the CSF of PMS patients are consistent with demyelination, which is a hallmark of MS.

Hypoxanthine was decreased, but inosine was increased in the CSF from PMS patients. Nucleotide and purine salvage pathways utilize these metabolites. Inosine is converted to hypoxanthine, which is further processed to xanthine. Therefore, an accumulation in the precursor inosine is consistent with a decrease in both hypoxanthine and xanthine. This is evident of an overall change in the activity of the rate-limiting enzyme in purine degradation, xanthine oxidase, which produces free radicals that can inhibit the neuronal uptake of glutamate and enhance glutamate-mediated excitotoxicity.[55] The observed decrease in glutamate may also explain the resulting down-regulation in xanthine oxidase activity.[56]

Creatine and urea were also observed to be perturbed in the CSF of PMS patients, but their relationship to the pathogenesis of MS is not clear. Creatine is irreversibly converted to creatinine. Our observation that creatinine levels were increased and creatine levels were decreased suggests this conversion is up-regulated in PMS patients, which is consistent with prior observations that creatine metabolism is dysfunctional in MS.[57] Urea has been identified as a variable metabolite in CSF, but its relationship to MS is controversial.[43]

MS-Induced Metabolic Alterations in Serum Mimics CSF. The metabolic changes in the serum of PMS patients were similar to the alterations observed in CSF and can be linked to the same MS-related pathologies. Like CSF, the 31 metabolites altered in serum (Table S1) were related to glycolysis and amino acid metabolism. Tyrosine was decreased in PMS serum, while phenylalanine and tryptophan were increased. These aromatic amino acids are precursors to neurotransmitters. Arginine, which is positively correlated with brain atrophy and white matter lesions, was found to be decreased in the serum from PMS patients.[58] Consistent with this decrease was the observation that the level of ornithine, which is downstream of arginine in the urea cycle, was increased. Creatine, whose biosynthesis also relies on arginine metabolism, was similarly found to be increased in the serum from PMS patients. Methionine is also positively correlated with brain atrophy and was similarly found to be increased in the serum from PMS patients.[59] Notably, methionine has been shown to be corelated with creatine biosynthesis, completing the metabolic connection between these four amino acids.[60]

https://doi.org/10.1021/acschemneuro.3c00678
ACS Chem. Neurosci. 2024, 15, 1110−1124

Asparagine, glutamine, and threonine were all found to be increased in the serum from PMS patients. Conversely, glutamate was decreased. As with CSF, BCAAs were similarly dysregulated in serum, with isoleucine increasing in PMS while leucine and valine were both decreased. Degradation products of BCAAs were again identified, with methylmalonate, 3-hydroxyisovalerate and 3-HB all being decreased in PMS. 3-Hydroxyisobutyrate, an intermediate in valine metabolism, was found to increase in PMS, which is consistent with the observed decrease in valine. Changes to purine metabolism and salvage pathways were again evident in the serum of PMS patients, as evidenced by an increase in guanine and inosine. Similarly, alterations in pyrimidine metabolism were evident in uracil. Of note, the increase in threonine is consistent with its potential to protect against peripheral neuropathy and reduce spasticity.[61,62]

In contrast to CSF, glucose was decreased and lactate was increased in the serum from PMS patients. Conversely, the level of alanine was decreased in serum, which was consistent with the CSF findings. Presumably, any available glucose was redirected to the brain to meet its needs.[63,64] Of course, this likely contributed to the observed buildup of glucose in the CSF due to the dysregulated glycolysis. Lactate has also been implicated as a major energy source for neurons, equivalent to glucose, and has been shown to be metabolized through the TCA cycle.[65−68] The proposed astrocyte-neuron lactate shuttle hypothesis (ANLSH)[69,70] suggests a major metabolic role and source of lactate in neurons from astrocytic glycolysis. Like glucose, lactate can easily cross the blood−brain barrier and is rapidly released from the brain into the blood.[71,72] Notably, elevated lactate levels in the blood have been previously identified following traumatic brain injury[73] or in the serum of MS patients.[74] Elevated lactate levels in the CSF have also been previously observed in Alzheimer's disease,[75] MS,[76] and Parkinson's disease.[77] Overall, neurological diseases are broadly associated with dysregulated glycolysis and changes in the concentrations of the associated metabolites.

Choline was found to be increased in PMS serum, is important in lipid synthesis, and enhances myelin repair. Glycerol is important in phospholipid biosynthesis and was found to decrease in serum. Myoinositol, a vital component of myelin, was also likely perturbed in the serum of PMS patients. Taken together, these dysregulated metabolites all suggest an impaired myelin repair system and may indicate lipogenic breakdown.[78] This observation is consistent with the demyelination that is common in PMS and the metabolic changes observed in the CSF.

Two metabolites, hippurate and niacinamide, were increased in the serum from PMS patients, which can be attributed to diet and medication. Imidazole, a precursor to histidine, was increased in the serum of PMS patients.

Metabolic Changes Implicate Pathways Linked to Neurodegeneration and Disease Progression. Three metabolites were found to consistently change in serum between Ctrl, RRMS, and PMS-B patients (Figure 4D). These metabolites include 3-HB, methylmalonate, and asparagine. Please note that some of these metabolic trends may differ when considering the entire PMS cohort (Table S1) compared to just the PMS-B subset. 3-HB consistently increased from Ctrl to RRMS to PMS-B. 3-HB serves multiple neuroprotective roles, including providing energy under glucose deprivation and limiting ROS.[47] Asparagine showed the opposite trend, decreasing from Ctrl to RRMS to PMS-B. A decrease in asparagine has been associated with impaired lipogenesis.[79] Methylmalonate shows differential changes with a modest increase from Ctrl to RRMS, but then a decrease in PMS-B, where PMS-B patients present lower levels of methylmalonate than Ctrl. Methylmalonate is a product of vitamin B12 metabolism and has been shown to be neurotoxic.[80] The increased levels from Ctrl to RRMS, followed by a decrease in RRMS to PMS-B, may indicate neuronal damage in the early stages of MS. These three metabolites may offer a unique approach to monitoring the onset of MS relative to healthy controls and disease progression from RRMS to PMS. One metabolite, thiamine pyrophosphate (TPP), was found to increase from RRMS to PMS-B patients but was not altered between PMS-B and Ctrl. TPP is necessary for glycolysis, oxidative phosphorylation, and the decarboxylation of BCAAs.[81] TPP may provide a unique biomarker of the progression from RRMS to PMS.

Urinary Metabolic Changes Are Consistent between MS Patients and Mouse MS Model. We have previously reported on the potential discovery of MS biomarkers using the NMR metabolomics analysis of urine samples collected from an experimental autoimmune encephalomyelitis (EAE)-mouse model and human patients diagnosed with RRMS.[36,37] The EAE-mouse model yielded 31 metabolites, and the human urine yielded 23 metabolites as potential biomarkers of MS. Only 6 of these metabolites were consistently detected between the two studies. Herein, we identified 14 metabolites in the urine of PMS patients that were altered relative to those of healthy controls. Combining the results from these three very distinct studies, two consistently detected metabolites were 3-HB and creatinine.

Five additional metabolites detected from the PMS urine samples were also partly consistent with our prior analysis of the urine samples from RRMS patients but not the EAE-mouse model. These metabolites include 3-hydroxyisovalerate, acetate, alanine, citrate, and phenylalanine. Phenylalanine was increased in both the serum and urine samples collected from PMS patients and in the prior RRMS urine samples. Alanine was decreased in both the CSF and serum samples collected from PMS patients and in the prior RRMS urine samples. It was increased in the PMS urine samples. Similarly, acetate was increased in both the PMS and prior RRMS urine samples but decreased in the PMS CSF samples. 3-Hydroxyisovalerate was also increased in both the PMS and prior RRMS urine samples but decreased in the PMS serum samples. Conversely, citrate was decreased in the urine from PMS and prior RRMS urine samples but was increased in the CSF.

Seven additional metabolites were differentially altered in the PMS urine samples relative to healthy controls that were not identified by our previous study with RRMS. This may be attributed to the later stage of MS disease in our PMS urine samples compared with RRMS. These additional PMS metabolites included arginine, indoxyl sulfate, and leucine, which were increased in the urine from PMS patients. Ascorbate, histidine, methyl nicotinamide, and trigonelline were decreased. Arginine was also decreased in PMS serum samples, while leucine was decreased in both serum and CSF. Histidine serves as a precursor to the neurotransmitter histamine and is important in ROS scavenging. Indoxyl sulfate may be a result of tryptophan degradation, which is also a precursor to neurotransmitters and may be indicative of brain function and psychiatric disorders.[82] Methyl nicotinamide is proposed to have neuroprotective potential in neurodegener-

https://doi.org/10.1021/acschemneuro.3c00678
ACS Chem. Neurosci. 2024, 15, 1110−1124

ative disease.[83] Again, the consistency across multiple biofluids and the association with MS pathogenesis provide support for these urinary metabolites as potential biomarkers for disease progression from RRMS to PMS.

Metabolic Changes across Multiple Biofluids Suggest Robust MS Biomarkers. Four metabolites were identified as consistently changing across the CSF, serum, and urine samples obtained from PMS patients (Figure 5). For clarity, the paired-matched [*i.e.*, CSF/serum (N = 57) and serum/urine (N = 46)] PMS cohort (Table 1) was used in this comparison. These metabolites include 3-HB, alanine, leucine, and phenylalanine. Notably, all four metabolites have a consistent fold-change pattern across the CSF (decrease) and urine (increase) relative to healthy controls. The metabolites displayed a partly random response to PMS in serum. 3-HB, alanine, and leucine were all decreased, while in contrast, the phenylalanine levels increased. It is important to note that 3-HB exhibits a reversed, increased trend in the serum (Figure 4D) when only the subset PMS-B (N = 48) cohort was used. Recall that the subset PMS-B cohort (Figure 4B) presents a larger metabolic difference than the pair-matched PMS cohort (Figures 2B,C and 5) or the subset PMS-A (Figure 4A) relative to healthy controls, which explains the 3-HB trend reversal. 3-HB serves as an alternative fuel source under glucose deprivation in the CNS and is vital for protection against inflammation and oxidative stress, for increasing cerebral blood flow, and for promoting the expression of neurotrophic factors.[47] The decreased levels of 3-HB in CSF were paired with a decrease in serum and an increase in urine, which may suggest a ketogenic state for MS patients. A shift from dysregulated glycolysis would result in the brain consuming higher levels of ketone bodies to compensate for the loss of glucose-derived energy.

The amino acids alanine, leucine, and phenylalanine all play important roles in CNS neurochemistry. A decrease in alanine in the CSF may indicate that it is metabolized to generate pyruvate to circumvent the decrease in glucose availability. Leucine is important for the synthesis of glutamate, which is a vital neurotransmitter that is necessary for regulating oxidative stress.[84] Phenylalanine is a precursor in dopamine synthesis, where decreased levels of dopamine are linked to fatigue or to the dopamine imbalance hypothesis.[85] Dopamine has been implicated as having a critical role in modulating the neuro-immune network that is important to MS pathogenesis.[86] The elevation of phenylalanine in the blood is also indicative of hypomyelination of neurons in mouse models.[87] Overall, the decreased levels of these amino acids in the CSF, which are all vital to neurological processes, suggest a lack of proper amino acid utilization by the CNS of MS patients.

The individual attributes of these four metabolites to MS pathogenesis and the fact that we detected statistically significant changes for these metabolites in all three biofluids relative to healthy controls offer significant promise for their potential as biomarkers of MS diagnosis and progression. Historically, there have been limited efforts to identify and explore metabolites across multiple biofluids as potential biomarkers of MS.[23,27,28] This lack of information about the dysregulation of metabolites across multiple locations throughout the human body may hinder our understanding of the development and progression of MS. A clearer association of metabolites and metabolic processes with MS pathology may become more evident as further multibiofluid studies are completed.

CONCLUSIONS

We identified potentially unique biomarkers of MS that were detected across three biofluids (*i.e.*, CSF, serum, and urine) obtained from patients diagnosed with progressive or RRMS. We identified four metabolites (*i.e.*, 3-HB, alanine, leucine, and phenylalanine) that may serve as multibiofluid biomarkers of PMS. Similarly, we detected three metabolites (*i.e.*, 3-HB, asparagine, and methylmalonate) that were found to change consistently (increase or decrease) as the disease progressed from healthy controls through RRMS to PMS. Thus, these metabolites may serve as biomarkers of MS disease progression. Our results were compared with our prior NMR metabolomics studies of urine samples collected from EAE-mice and RRMS patients and identified two urine metabolites detected across all three studies.[36,37] Thus, 3-HB and creatinine from human urine samples may serve as readily accessible, quick, easy, and noninvasive diagnostic markers of MS. Excluding the EAE-mouse study from the comparison resulted in the identification of five additional urinary metabolites (*i.e.*, 3-hydroxyisovalerate, acetate, alanine, citrate, and phenylalanine) that may further serve as MS biomarkers. Similarly, seven metabolites (*i.e.*, arginine, histidine, indoxyl sulfate, leucine, methyl nicotinamide, and trigonelline) were detected only in the urine of PMS patients and not in RRMS patients, which may be useful urine biomarkers of MS progression. In addition to being detected across multiple biofluids and by multiple studies, these metabolites can be linked to numerous biological processes associated with MS pathology. Eleven of these metabolites have also been identified by other clinical metabolomics studies as potential MS biomarkers (Table S2). In total, we present robust evidence of the reliability and utility of these metabolites to serve as potential biomarkers for MS diagnosis and disease progression. Few prior studies have successfully identified a set of metabolites that consistently varied across multiple biofluids.[88−90] By identification of unique biomarkers across multiple biofluids, the mechanisms of MS physiology may be better understood. Further, a unique and robust set of metabolite biomarkers for rapid and differential diagnosis of MS as well as for monitoring the effectiveness of MS treatment may be achieved.

The treatment of MS is challenged by the lack of a cure and the existence of four disease courses: clinically isolated syndrome (CIS), RRMS, secondary progressive (SPMS), and primary progressive (PPMS). Thus, current MS therapies seek to decrease the progression and severity of the disease while also providing relief to patient symptoms. There are over 20 different U.S. Food and Drug Administration (FDA)-approved disease-modifying treatments (DMT) for MS, where there are more treatment choices for RRMS than PMS.[91] A particular patient's choice of DMT is based on a balance of maximizing efficacy (*i.e.*, decreasing disease progression) while avoiding or minimizing side-effects (*i.e.*, bruising easily, flu-like symptoms, heart palpitations, increased risk of infections, *etc.*). Accordingly, it is common for MS patients to change their DMT multiple times throughout the course of their treatment, especially as the disease enters distinct stages. Thus, in addition to helping diagnose and prognose MS, the potential metabolite biomarkers outlined above may assist in providing personalized care by aiding a physician in identifying a proper DMT for a given patient. As an illustrative example, a patient who only presents the four PMS metabolites (*i.e.*, 3-HB, alanine, leucine,

https://doi.org/10.1021/acschemneuro.3c00678
ACS Chem. Neurosci. 2024, 15, 1110−1124

and phenylalanine) in either of the three biofluids or the seven metabolites (*i.e.*, 3-hydroxyisovalerate, arginine, histidine, indoxyl sulfate, leucine, methyl nicotinamide, and trigonelline) in only urine may suggest a physician consider beginning a MS treatment with ocrelizumab.[92] Conversely, a MS patient receiving a typical first-line therapy (*e.g.*, dimethyl fumarate, fingolimod, glatiramer acetate, interferon β 1*b*/1*a*, or teriflunomide) but starting to demonstrate changes in the three metabolites associated with a progression from RRMS to PMS (*i.e.*, 3-HB, asparagine, and methylmalonate) may suggest a physician consider initiating a transition to a second-line treatment (*e.g.*, natalizumab) or even a third-line treatment (*e.g.*, alemtuzumab).[91] Finally, a new MS patient that does not demonstrate either the PMS or the progression from RRMS to PMS metabolite biomarkers listed above but instead exhibits the six consistently detected urinary MS metabolites (*i.e.*, 3-HB, acetate, alanine, citrate, creatinine, and phenylalanine) may inform a physician to consider starting the patient with typical first-line MS therapy. Factors that inform a clinician to start or change a treatment for MS are limited and are often dependent on few evidence-based data, observational reports, and practical experience. The ready accessibility of metabolite biomarkers that can simplify the assessment of MS disease progression and a patient's response to treatment would simplify a clinician's decision process and lead to better outcomes for the MS patient.

Despite the potential utility and promise of our results, there are still several caveats that need to be addressed before these metabolites can be accurately labeled as biomarkers of MS. Foremost is the need to further validate these potential biomarkers with additional clinical studies. In addition, it is still plausible that confounding factors, such as the type of drug treatment or a generic response to a disease state (*i.e.*, immune response), may explain the observed metabolic difference between MS patients and healthy controls. The metabolic changes could also reflect common symptoms or comorbidities of MS like obesity, diabetes, depression, and cardiovascular diseases, among other issues. Another consideration is the possibility that the metabolic response is not unique to MS and is observed in other neurological, autoimmune, or diseases in general. Nevertheless, an important advantage of metabolomic-based biomarkers is the identification of a set of metabolites instead of a typical single molecular biomarker. While individual metabolites may be associated with other disease states besides MS, it is still likely that the full set of metabolites, in addition to the relative trends (*i.e.*, increase or decrease), may be uniquely attributed to MS and serve as a viable biomarker for disease diagnosis, progression, and personalized medicine.

MATERIALS AND METHODS

Study Design and Cohort Demographics. The aim of this study was to track metabolites across multiple biofluids that were acquired from MS patients and healthy volunteers without a MS diagnosis. We received CSF, serum, and urine samples from the NIH NeuroBioBank, which included the University of Maryland Brain and Tissue Bank, the University of Miami Brain Endowment Bank, and the Human Brain and Spinal Fluid Resource Center. To supplement the NIH NeuroBioBank samples, we collected additional biofluids at the MS clinic within the Saunders Medical Center (Wahoo, NE, USA). Specifically, serum and urine samples were collected from RRMS patients during their normal healthcare visits and from healthy family members. All materials, biospecimens, and human subjects' data collected, stored, and maintained for and during the conduct of this research was reviewed and approved by the University of Nebraska-Lincoln Institutional Review Board (IRB, IRB#: 20200820533EP and IRB#: 20180517991EPCOLLA). Limited human subject data were available for all biospecimens provided by the NIH NeuroBioBank and primarily consisted of age, sex, biofluid type, and MS classification. The type of treatment received by the MS patient was only provided by the Saunders Medical Center and corresponded to a range of options consisting of Avonex (3.8%), Copaxone (3.8%), Ocrevus (5.8%), Plegridy (1.9%), Tecfidera (34.6%), Tysabri (46.2%), or none (3.8%). A complete description of the cohorts used in this study is provided in Table 1. Briefly, we received a total of 73 CSF, 44 serum, and 39 urine samples from healthy controls; and 99 CSF, 248 serum, and 154 urine samples from MS patients. We focused our NMR metabolomics analyses on sets of patient samples in which we had access to at least two types of biofluids from the same patient. For example, a serum sample paired with either a CSF or urine sample acquired from the same patient was included in the set of biofluid samples used to acquire a NMR spectrum for biomarker identification. Biofluid samples were excluded from further analysis if the sample did not yield a high-quality NMR spectrum or the spectral data were outliers in an initial PCA score plot. Of the total number of samples received from the NIH NeuroBioBank and Saunders Medical Center, a reduced subset of each biofluid was used in the NMR metabolomics analyses, as denoted by the numbers in parentheses in Table 1. These sample subsets were closely matched for age and sex. In total, 96 CSF, 183 serum, and 72 urine samples were used in the metabolomics NMR data analyses.

Our NMR metabolomics experiments followed our standard procedures as previously published.[93,94] Experimental details of the NMR sample preparation, NMR data collection and processing, and univariate and multivariate statistical analysis are provided in Supporting Information.

ASSOCIATED CONTENT

Supporting Information

The Supporting Information is available free of charge at https://pubs.acs.org/doi/10.1021/acschemneuro.3c00678.

Experimental details, materials, and methods that describe CSF, serum, and urine sample preparations for NMR analysis; NMR data collection, processing, and statistical analysis protocols; box and whisker plots of additional metabolite alterations in CSF, serum, and urine in PMS patient samples; metabolites from serum samples pair-matched with CSF samples; urine samples pair-matched with serum samples; list of assigned metabolites and their associated experimental data; and comparison of potential MS metabolites identified by this study with the literature (PDF)

AUTHOR INFORMATION

Corresponding Author

Robert Powers − *Department of Chemistry, University of Nebraska-Lincoln, Lincoln, Nebraska 68588-0304, United States; Nebraska Center for Integrated Biomolecular Communication, University of Nebraska-Lincoln, Lincoln, Nebraska 68588-0304, United States;* orcid.org/0000-0001-9948-6837; Phone: (402) 472-3039; Email: rpowers3@unl.edu; Fax: (402) 472-9402

Authors

Fatema Bhinderwala − *Department of Chemistry, University of Nebraska-Lincoln, Lincoln, Nebraska 68588-0304, United States; Nebraska Center for Integrated Biomolecular Communication, University of Nebraska-Lincoln, Lincoln, Nebraska 68588-0304, United States;* Present

Address: University of Pittsburgh School of Medicine, Department of Structural Biology, Pittsburgh, PA 15213
Heidi E. Roth − *Department of Chemistry, University of Nebraska-Lincoln, Lincoln, Nebraska 68588-0304, United States*
Mary Filipi − *Multiple Sclerosis Clinic, Saunders Medical Center, Wahoo, Nebraska 68066, United States*
Samantha Jack − *Multiple Sclerosis Clinic, Saunders Medical Center, Wahoo, Nebraska 68066, United States*

Complete contact information is available at: https://pubs.acs.org/10.1021/acschemneuro.3c00678

Author Contributions

F.B. and H.E.R. contributed equally to the work. R.P. conceived the project. R.P., S.J., and M.F. obtained funding and I.R.B. approval for the study. F.B. prepared all samples and collected the dataset and H.R. and F.B. analyzed the data. H.R., F.B., and R.P. wrote and edited the manuscript.

Notes

The authors declare no competing financial interest.

■ ACKNOWLEDGMENTS

We would like to thank the NIH NeuroBioBank, the University of Maryland Brain and Tissue Bank, the University of Miami Brain Endowment Bank, and the Human Brain and Spinal Fluid Resource Center (HBSFRC) for providing the CSF, serum, and urine samples used in this study. We would also like to thank Dr. Martha Morton, Director of the Molecular Analysis and Characterization Facility within the Department of Chemistry at the University of Nebraska-Lincoln for her assistance in acquiring NMR data. This work was funded by a grant (0070) from the Paralyzed Veterans of America and, in part, from the Nebraska Center for Integrated Biomolecular Communication (P20 GM113126, NIGMS). The research was performed in facilities renovated with support from the National Institutes of Health (RR015468-01).

■ REFERENCES

(1) Wallin, M. T.; Culpepper, W. J.; Campbell, J. D.; Nelson, L. M.; Langer-Gould, A.; Marrie, R. A.; Cutter, G. R.; Kaye, W. E.; Wagner, L.; Tremlett, H.; et al. The prevalence of MS in the United States. *Neurology* **2019**, *92* (10), No. e1029.
(2) Dobson, R.; Giovannoni, G. Multiple sclerosis - a review. *Eur. J. Neurol.* **2019**, *26* (1), 27−40.
(3) Ghasemi, N.; Razavi, S.; Nikzad, E. Multiple Sclerosis: Pathogenesis, Symptoms, Diagnoses and Cell-Based Therapy. *J. Cell.* **2017**, *19* (1), 1−10.
(4) Krupp, L. B.; Rizvi, S. A. Symptomatic therapy for underrecognized manifestations of multiple sclerosis. *Neurology* **2002**, *58*, S32−S39.
(5) Brownlee, W. J.; Hardy, T. A.; Fazekas, F.; Miller, D. H. Diagnosis of multiple sclerosis: progress and challenges. *Lancet* **2017**, *389* (10076), 1336−1346.
(6) Thompson, A. J.; Banwell, B. L.; Barkhof, F.; Carroll, W. M.; Coetzee, T.; Comi, G.; Correale, J.; Fazekas, F.; Filippi, M.; Freedman, M. S.; et al. Diagnosis of multiple sclerosis: 2017 revisions of the McDonald criteria. *Lancet Neurol.* **2018**, *17* (2), 162−173.
(7) Rolak, L. A.; Fleming, J. O. The differential diagnosis of multiple sclerosis. *Neurologist* **2007**, *13*, 57−72.
(8) Hahn, J. S.; Pohl, D.; Rensel, M.; Rao, S. Differential diagnosis and evaluation in pediatric multiple sclerosis. *Neurology* **2007**, *68*, S13−S22.
(9) Fadil, H.; Kelley, R. E.; Gonzalez-Toledo, E. Differential diagnosis of multiple sclerosis. *Int. Rev. Neurobiol.* **2007**, *79*, 393−422.
(10) Lassmann, H.; Bruck, W.; Lucchinetti, C. Heterogeneity of multiple sclerosis pathogenesis: implications for diagnosis and therapy. *Trends Mol. Med.* **2001**, *7* (3), 115−121.
(11) Thompson, A. J.; Banwell, B. L.; Barkhof, F.; Carroll, W. M.; Coetzee, T.; Comi, G.; Correale, J.; Fazekas, F.; Filippi, M.; Freedman, M. S.; et al. Diagnosis of multiple sclerosis: 2017 revisions of the McDonald criteria. *Lancet Neurol.* **2018**, *17*, 162−173.
(12) Wildner, P.; Stasiołek, M.; Matysiak, M. Differential diagnosis of multiple sclerosis and other inflammatory CNS diseases. *Mult. Scler. Relat. Disord.* **2020**, *37*, 101452.
(13) Miller, J. R. The importance of early diagnosis of multiple sclerosis. *J. Manag. Care Pharm.* **2004**, *10* (3 Suppl B), S4−S11.
(14) Bates, D. Treatment effects of immunomodulatory therapies at different stages of multiple sclerosis in short-term trials. *Neurology* **2011**, *76* (1_supplement_1), S14−S25.
(15) Noyes, K.; Weinstock-Guttman, B. Impact of diagnosis and early treatment on the course of multiple sclerosis. *Am. J. Manag. Care* **2013**, *19* (17), s321−s331.
(16) Anlar, O. Treatment of multiple sclerosis. *CNS Neurol. Disord.: Drug Targets* **2009**, *8*, 167−174.
(17) Leray, E.; Yaouanq, J.; Le Page, E.; Coustans, M.; Laplaud, D.; Oger, J.; Edan, G. Evidence for a two-stage disability progression in multiple sclerosis. *Brain* **2010**, *133* (7), 1900−1913.
(18) Tolstikov, V.; Moser, A. J.; Sarangarajan, R.; Narain, N. R.; Kiebish, M. A. Current Status of Metabolomic Biomarker Discovery: Impact of Study Design and Demographic Characteristics. *Metabolites* **2020**, *10* (6), 224.
(19) Davillas, A.; Pudney, S. Using biomarkers to predict healthcare costs: Evidence from a UK household panel. *J. Health Econ.* **2020**, *73*, 102356.
(20) Hassan-Smith, G.; Wallace, G. R.; Douglas, M. R.; Sinclair, A. J. The role of metabolomics in neurological disease. *J. Neuroimmunol.* **2012**, *248* (1−2), 48−52.
(21) Zahoor, I.; Rui, B.; Khan, J.; Datta, I.; Giri, S. An emerging potential of metabolomics in multiple sclerosis: a comprehensive overview. *Cell. Mol. Life Sci.* **2021**, *78* (7), 3181−3203.
(22) Yan, J.; Kuzhiumparambil, U.; Bandodkar, S.; Dale, R. C.; Fu, S. Cerebrospinal fluid metabolomics: detection of neuroinflammation in human central nervous system disease. *Clin. Transl. Immunol.* **2021**, *10* (8), No. e1318.
(23) Rispoli, M. G.; Valentinuzzi, S.; De Luca, G.; Del Boccio, P.; Federici, L.; Di Ioia, M.; Digiovanni, A.; Grasso, E. A.; Pozzilli, V.; Villani, A.; et al. Contribution of Metabolomics to Multiple Sclerosis Diagnosis, Prognosis and Treatment. *Int. J. Mol. Sci.* **2021**, *22* (20), 11112.
(24) Polman, C. H.; Reingold, S. C.; Banwell, B.; Clanet, M.; Cohen, J. A.; Filippi, M.; Fujihara, K.; Havrdova, E.; Hutchinson, M.; Kappos, L.; et al. Diagnostic criteria for multiple sclerosis: 2010 revisions to the McDonald criteria. *Ann. Neurol.* **2011**, *69* (2), 292−302.
(25) Wright, B. L. C.; Lai, J. T. F.; Sinclair, A. J. Cerebrospinal fluid and lumbar puncture: a practical review. *J. Neurol.* **2012**, *259* (8), 1530−1545.
(26) Jafari, A.; Babajani, A.; Rezaei-Tavirani, M. Multiple Sclerosis Biomarker Discoveries by Proteomics and Metabolomics Approaches. *Biomark. Insights* **2021**, *16*, 117727192110133.
(27) Porter, L.; Shoushtarizadeh, A.; Jelinek, G. A.; Brown, C. R.; Lim, C. K.; de Livera, A. M.; Jacobs, K. R.; Weiland, T. J. Metabolomic Biomarkers of Multiple Sclerosis: A Systematic Review. *Front. Mol. Biosci.* **2020**, *7*, 574133.
(28) Liu, Z.; Waters, J.; Rui, B. Metabolomics as a promising tool for improving understanding of multiple sclerosis: A review of recent advances. *Biomed. J.* **2022**, *45* (4), 594−606.
(29) Zhang, A.; Sun, H.; Wang, X. Serum metabolomics as a novel diagnostic approach for disease: a systematic review. *Anal. Bioanal. Chem.* **2012**, *404* (4), 1239−1245.
(30) Zhang, A.; Sun, H.; Wu, X.; Wang, X. Urine metabolomics. *Clin. Chim. Acta* **2012**, *414*, 65−69.

(31) Wang, T.; Tang, L.; Lin, R.; He, D.; Wu, Y.; Zhang, Y.; Yang, P.; He, J. Individual variability in human urinary metabolites identifies age-related, body mass index-related, and sex-related biomarkers. *Mol. Genet. Genomic Med.* **2021**, *9* (8), No. e1738.
(32) Jing, J.; Gao, Y. Urine biomarkers in the early stages of diseases: current status and perspective. *Discov. Med.* **2018**, *25* (136), 57−65.
(33) Roth, H. E.; Powers, R. Meta-Analysis Reveals Both the Promises and the Challenges of Clinical Metabolomics. *Cancers* **2022**, *14* (16), 3992.
(34) Goveia, J.; Pircher, A.; Conradi, L.-C.; Kalucka, J.; Lagani, V.; Dewerchin, M.; Eelen, G.; DeBerardinis, R. J.; Wilson, I. D.; Carmeliet, P. Meta-analysis of clinical metabolic profiling studies in cancer: challenges and opportunities. *EMBO Mol. Med.* **2016**, *8* (10), 1134−1142.
(35) Morze, J.; Wittenbecher, C.; Schwingshackl, L.; Danielewicz, A.; Rynkiewicz, A.; Hu, F. B.; Guasch-Ferré, M. Metabolomics and Type 2 Diabetes Risk: An Updated Systematic Review and Meta-analysis of Prospective Cohort Studies. *Diabetes Care* **2022**, *45* (4), 1013−1024.
(36) Gebregiworgis, T.; Massilamany, C.; Gangaplara, A.; Thulasingam, S.; Kolli, V.; Werth, M. T.; Dodds, E. D.; Steffen, D.; Reddy, J.; Powers, R. Potential of Urinary Metabolites for Diagnosing Multiple Sclerosis. *ACS Chem. Biol.* **2013**, *8* (4), 684−690.
(37) Gebregiworgis, T.; Nielsen, H. H.; Massilamany, C.; Gangaplara, A.; Reddy, J.; Illes, Z. L.; Powers, R. A Urinary Metabolic Signature for Multiple Sclerosis and Neuromyelitis Optica. *J. Proteome Res.* **2016**, *15* (2), 659−666.
(38) Bauernfeind, A. L.; Barks, S. K.; Duka, T.; Grossman, L. I.; Hof, P. R.; Sherwood, C. C. Aerobic glycolysis in the primate brain: reconsidering the implications for growth and maintenance. *Brain Struct. Funct.* **2014**, *219* (4), 1149−1167.
(39) Brière, J. J.; Favier, J.; Gimenez-Roqueplo, A.-P.; Rustin, P. Tricarboxylic acid cycle dysfunction as a cause of human diseases and tumor formation. *Am. J. Physiol. Cell Physiol.* **2006**, *291* (6), C1114−C1120.
(40) Yan, X.; Hu, Y.; Wang, B.; Wang, S.; Zhang, X. Metabolic Dysregulation Contributes to the Progression of Alzheimer's Disease. *Front. Neurosci.* **2020**, *14*, 530219.
(41) Zhang, S.; Zhang, Y.; Wen, Z.; Yang, Y.; Bu, T.; Bu, X.; Ni, Q. Cognitive dysfunction in diabetes: abnormal glucose metabolic regulation in the brain. *Front. Endocrinol.* **2023**, *14*, 1192602.
(42) Lai, J.-q.; Shi, Y.-C.; Lin, S.; Chen, X.-R. Metabolic disorders on cognitive dysfunction after traumatic brain injury. *Trends Endocrinol. Metabol.* **2022**, *33* (7), 451−462.
(43) Sinclair, A. J.; Viant, M. R.; Ball, A. K.; Burdon, M. A.; Walker, E. A.; Stewart, P. M.; Rauz, S.; Young, S. P. NMR-based metabolomic analysis of cerebrospinal fluid and serum in neurological diseases-a diagnostic tool? *NMR Biomed.* **2010**, *23* (2), 123−132.
(44) Kim, H.-H.; Jeong, I. H.; Hyun, J.-S.; Kong, B. S.; Kim, H. J.; Park, S. J. Metabolomic profiling of CSF in multiple sclerosis and neuromyelitis optica spectrum disorder by nuclear magnetic resonance. *PLoS One* **2017**, *12* (7), No. e0181758.
(45) Holeček, M. Branched-chain amino acids in health and disease: metabolism, alterations in blood plasma, and as supplements. *Nutr. Metabol.* **2018**, *15*, 33.
(46) Ikeda, K.; Kinoshita, M.; Kayama, H.; Nagamori, S.; Kongpracha, P.; Umemoto, E.; Okumura, R.; Kurakawa, T.; Murakami, M.; Mikami, N.; et al. Slc3a2Mediates Branched-Chain Amino-Acid-Dependent Maintenance of Regulatory T Cells. *Cell Rep.* **2017**, *21* (7), 1824−1838.
(47) Møller, N. Ketone Body, 3-Hydroxybutyrate: Minor Metabolite - Major Medical Manifestations. *J. Clin. Endocrinol. Metab.* **2020**, *105* (9), 2884−2892.
(48) Schmieden, V.; Kuhse, J.; Betz, H. A Novel Domain of the Inhibitory Glycine Receptor Determining Antagonist Efficacies: Further Evidence for Partial Agonism Resulting from Self-Inhibition. *Mol. Pharmacol.* **1999**, *56* (3), 464−472.
(49) Long, P. M.; Moffett, J. R.; Namboodiri, A. M. A.; Viapiano, M. S.; Lawler, S. E.; Jaworski, D. M. N-acetylaspartate (NAA) and N-acetylaspartylglutamate (NAAG) promote growth and inhibit differentiation of glioma stem-like cells. *J. Biol. Chem.* **2013**, *288* (36), 26188−26200.
(50) Rowley, N. M.; Madsen, K. K.; Schousboe, A.; Steve White, H. Glutamate and GABA synthesis, release, transport and metabolism as targets for seizure control. *Neurochem. Int.* **2012**, *61* (4), 546−558.
(51) Matés, J. M.; Pérez-Gómez, C.; de Castro, I. N.; Asenjo, M.; Márquez, J. Glutamine and its relationship with intracellular redox status, oxidative stress and cell proliferation/death. *Int. J. Biochem. Cell Biol.* **2002**, *34* (5), 439−458.
(52) Lou, H. C. Dopamine precursors and brain function in phenylalanine hydroxylase deficiency. *Acta Paediatr. Suppl.* **1994**, *83*, 86−88.
(53) Salway, J. G.; Finnegan, J.; Barnett, D.; Whitehead, L.; Karunanayaka, A.; Payne, R. B. Effect of myo-inositol on peripheral-nerve function in diabetes. *Lancet* **1978**, *312* (8103), 1282−1284.
(54) Sy, M.; Brandt, A. U.; Lee, S. U.; Newton, B. L.; Pawling, J.; Golzar, A.; Rahman, A. M. A.; Yu, Z.; Cooper, G.; Scheel, M.; et al. N-acetylglucosamine drives myelination by triggering oligodendrocyte precursor cell differentiation. *J. Biol. Chem.* **2020**, *295* (51), 17413−17424.
(55) Stover, J. F.; Lowitzsch, K.; Kempski, O. S. Cerebrospinal fluid hypoxanthine, xanthine and uric acid levels may reflect glutamate-mediated excitotoxicity in different neurological diseases. *Neurosci. Lett.* **1997**, *238* (1−2), 25−28.
(56) Singh, K.; Ahluwalia, P. Studies on the effect of monosodium glutamate (MSG) administration on the activity of xanthine oxidase, superoxide dismutase and catalase in hepatic tissue of adult male mice. *Indian J. Clin. Biochem.* **2002**, *17* (1), 29−33.
(57) Ostojic, S. M. Creatine and multiple sclerosis. *Nutr. Neurosci.* **2022**, *25* (5), 912−919.
(58) Kitamura, M.; Yatsuga, S.; Abe, T.; Povalko, N.; Saiki, R.; Ushijima, K.; Yamashita, Y.; Koga, Y. L-Arginine intervention at hyper-acute phase protects the prolonged MRI abnormality in MELAS. *J. Neurol.* **2016**, *263* (8), 1666−1668.
(59) Hooshmand, B.; Refsum, H.; Smith, A. D.; Kalpouzos, G.; Mangialasche, F.; von Arnim, C. A. F.; Kåreholt, I.; Kivipelto, M.; Fratiglioni, L. Association of Methionine to Homocysteine Status With Brain Magnetic Resonance Imaging Measures and Risk of Dementia. *JAMA Psychiatr.* **2019**, *76* (11), 1198−1205.
(60) Tang, X.; Keenan, M. M.; Wu, J.; Lin, C. A.; Dubois, L.; Thompson, J. W.; Freedland, S. J.; Murphy, S. K.; Chi, J. T. Comprehensive profiling of amino acid response uncovers unique methionine-deprived response dependent on intact creatine biosynthesis. *PLoS Genet.* **2015**, *11* (4), No. e1005158.
(61) Sun, Y.; Kim, J. H.; Vangipuram, K.; Hayes, D. F.; Smith, E. M. L.; Yeomans, L.; Henry, N. L.; Stringer, K. A.; Hertz, D. L. Pharmacometabolomics reveals a role for histidine, phenylalanine, and threonine in the development of paclitaxel-induced peripheral neuropathy. *Breast Cancer Res. Treat.* **2018**, *171* (3), 657−666.
(62) Hauser, S. L.; Doolittle, T. H.; Lopez-Bresnahan, M.; Shahani, B.; Schoenfeld, D.; Shih, V. E.; Growdon, J.; Lehrich, J. R. An antispasticity effect of threonine in multiple sclerosis. *Arch. Neurol.* **1992**, *49* (9), 923−926.
(63) Mangia, S.; Giove, F.; Tkáč, I.; Logothetis, N. K.; Henry, P. G.; Olman, C. A.; Maraviglia, B.; Di Salle, F.; Uğurbil, K. Metabolic and hemodynamic events after changes in neuronal activity: current hypotheses, theoretical predictions and in vivo NMR experimental findings. *J. Cereb. Blood Flow Metab. Suppl.* **2009**, *29* (3), 441−463.
(64) Mergenthaler, P.; Lindauer, U.; Dienel, G. A.; Meisel, A. Sugar for the brain: the role of glucose in physiological and pathological brain function. *Trends Neurosci.* **2013**, *36* (10), 587−597.
(65) Dembitskaya, Y.; Piette, C.; Perez, S.; Berry, H.; Magistretti, P. J.; Venance, L. Lactate supply overtakes glucose when neural computational and cognitive loads scale up. *Proc. Natl. Acad. Sci. U.S.A.* **2022**, *119* (47), No. e2212004119.
(66) Magistretti, P. J.; Allaman, I. Lactate in the brain: from metabolic end-product to signalling molecule. *Nat. Rev. Neurosci.* **2018**, *19* (4), 235−249.

https://doi.org/10.1021/acschemneuro.3c00678
ACS Chem. Neurosci. 2024, 15, 1110−1124

(67) Karagiannis, A.; Gallopin, T.; Lacroix, A.; Plaisier, F.; Piquet, J.; Geoffroy, H.; Hepp, R.; Naudé, J.; Le Gac, B.; Egger, R.; et al. Lactate is an energy substrate for rodent cortical neurons and enhances their firing activity. *Elife* **2021**, *10*, No. e71424.
(68) Pellerin, L. Lactate as a pivotal element in neuron-glia metabolic cooperation. *Neurochem. Int.* **2003**, *43* (4−5), 331−338.
(69) Barros, L. F.; Weber, B. CrossTalk proposal: an important astrocyte-to-neuron lactate shuttle couples neuronal activity to glucose utilisation in the brain. *J. Physiol.* **2018**, *596* (3), 347−350.
(70) Pellerin, L.; Magistretti, P. J. Glutamate uptake into astrocytes stimulates aerobic glycolysis: a mechanism coupling neuronal activity to glucose utilization. *Proc. Natl. Acad. Sci. U.S.A.* **1994**, *91* (22), 10625−10629.
(71) Knudsen, G. M.; Paulson, O. B.; Hertz, M. M. Kinetic analysis of the human blood-brain barrier transport of lactate and its influence by hypercapnia. *J. Cereb. Blood Flow Metab. Suppl.* **1991**, *11* (4), 581−586.
(72) Dienel, G. A. Brain lactate metabolism: the discoveries and the controversies. *J. Cereb. Blood Flow Metab. Suppl.* **2012**, *32* (7), 1107−1138.
(73) Cai, M.; Wang, H.; Song, H.; Yang, R.; Wang, L.; Xue, X.; Sun, W.; Hu, J. Lactate Is Answerable for Brain Function and Treating Brain Diseases: Energy Substrates and Signal Molecule. *Front. Nutr.* **2022**, *9*, 800901.
(74) Amorini, A. M.; Nociti, V.; Petzold, A.; Gasperini, C.; Quartuccio, E.; Lazzarino, G.; Di Pietro, V.; Belli, A.; Signoretti, S.; Vagnozzi, R.; et al. Serum lactate as a novel potential biomarker in multiple sclerosis. *Biochim. Biophys. Acta, Mol. Basis Dis.* **2014**, *1842* (7), 1137−1143.
(75) Liguori, C.; Chiaravalloti, A.; Sancesario, G.; Stefani, A.; Sancesario, G. M.; Mercuri, N. B.; Schillaci, O.; Pierantozzi, M. Cerebrospinal fluid lactate levels and brain [18F]FDG PET hypometabolism within the default mode network in Alzheimer's disease. *Eur. J. Nucl. Med. Mol. Imag.* **2016**, *43* (11), 2040−2049.
(76) Albanese, M.; Zagaglia, S.; Landi, D.; Boffa, L.; Nicoletti, C. G.; Marciani, M. G.; Mandolesi, G.; Marfia, G. A.; Buttari, F.; Mori, F.; et al. Cerebrospinal fluid lactate is associated with multiple sclerosis disease progression. *J. Neuroinflammation* **2016**, *13*, 36.
(77) Schirinzi, T.; Di Lazzaro, G.; Sancesario, G. M.; Summa, S.; Petrucci, S.; Colona, V. L.; Bernardini, S.; Pierantozzi, M.; Stefani, A.; Mercuri, N. B.; et al. Young-onset and late-onset Parkinson's disease exhibit a different profile of fluid biomarkers and clinical features. *Neurobiol. Aging* **2020**, *90*, 119−124.
(78) Frieler, R. A.; Mitteness, D. J.; Golovko, M. Y.; Gienger, H. M.; Rosenberger, T. A. Quantitative determination of free glycerol and myo-inositol from plasma and tissue by high-performance liquid chromatography. *J. Chromatogr. B: Anal. Technol. Biomed. Life Sci.* **2009**, *877* (29), 3667−3672.
(79) Xu, Y.; Shi, T.; Cui, X.; Yan, L.; Wang, Q.; Xu, X.; Zhao, Q.; Xu, X.; Tang, Q. Q.; Tang, H.; et al. Asparagine reinforces mTORC1 signaling to boost thermogenesis and glycolysis in adipose tissues. *EMBO J.* **2021**, *40* (24), No. e108069.
(80) Levin, J.; Bötzel, K.; Giese, A.; Vogeser, M.; Lorenzl, S. Elevated levels of methylmalonate and homocysteine in Parkinson's disease, progressive supranuclear palsy and amyotrophic lateral sclerosis. *Dement. Geriatr. Cogn. Disord* **2010**, *29* (6), 553−559.
(81) Lonsdale, D. A review of the biochemistry, metabolism and clinical benefits of thiamin(e) and its derivatives. *J. Evidence-Based Complementary Altern. Med.* **2006**, *3* (1), 49−59.
(82) Brydges, C. R.; Fiehn, O.; Mayberg, H. S.; Schreiber, H.; Dehkordi, S. M.; Bhattacharyya, S.; Cha, J.; Choi, K. S.; Craighead, W. E.; Krishnan, R. R.; et al. Indoxyl sulfate, a gut microbiome-derived uremic toxin, is associated with psychic anxiety and its functional magnetic resonance imaging-based neurologic signature. *Sci. Rep.* **2021**, *11* (1), 21011.
(83) Mu, R. H.; Tan, Y. Z.; Fu, L. L.; Nazmul Islam, M.; Hu, M.; Hong, H.; Tang, S. S. 1-Methylnicotinamide attenuates lipopolysaccharide-induced cognitive deficits via targeting neuroinflammation and neuronal apoptosis. *Int. Immunopharmacol.* **2019**, *77*, 105918.
(84) Sperringer, J. E.; Addington, A.; Hutson, S. M. Branched-Chain Amino Acids and Brain Metabolism. *Neurochem. Res.* **2017**, *42* (6), 1697−1709.
(85) Dobryakova, E.; Genova, H. M.; DeLuca, J.; Wylie, G. R. The dopamine imbalance hypothesis of fatigue in multiple sclerosis and other neurological disorders. *Front. Neurol.* **2015**, *6*, 52.
(86) Melnikov, M.; Pashenkov, M.; Boyko, A. Dopaminergic Receptor Targeting in Multiple Sclerosis: Is There Therapeutic Potential? *Int. J. Mol. Sci.* **2021**, *22* (10), 5313.
(87) Joseph, B.; Dyer, C. A. Relationship between myelin production and dopamine synthesis in the PKU mouse brain. *J. Neurochem.* **2003**, *86* (3), 615−626.
(88) Ellis, B.; Hye, A.; Snowden, S. G. Metabolic Modifications in Human Biofluids Suggest the Involvement of Sphingolipid, Antioxidant, and Glutamate Metabolism in Alzheimer's Disease Pathogenesis. *J. Alzheimer's Dis.* **2015**, *46* (2), 313−327.
(89) Graça, G.; Diaz, S. O.; Pinto, J.; Barros, A. S.; Duarte, I. F.; Goodfellow, B. J.; Galhano, E.; Pita, C.; Almeida, M. d. C.; Carreira, I. M.; et al. Can Biofluids Metabolic Profiling Help to Improve Healthcare during Pregnancy? *Spectros. Int. J.* **2012**, *27*, 128367.
(90) Yousri, N. A.; Mook-Kanamori, D. O.; Selim, M. M. E.-D.; Takiddin, A. H.; Al-Homsi, H.; Al-Mahmoud, K. A. S.; Karoly, E. D.; Krumsiek, J.; Do, K. T.; Neumaier, U.; et al. A systems view of type 2 diabetes-associated metabolic perturbations in saliva, blood and urine at different timescales of glycaemic control. *Diabetologia* **2015**, *58* (8), 1855−1867.
(91) Gajofatto, A.; Benedetti, M. D. Treatment strategies for multiple sclerosis: When to start, when to change, when to stop? *World J Clin Cases* **2015**, *3* (7), 545−555.
(92) Lin, M.; Zhang, J.; Zhang, Y.; Luo, J.; Shi, S. Ocrelizumab for multiple sclerosis. *Cochrane Database Syst. Rev.* **2022**, *2022* (5), Cd013247.
(93) Bhinderwala, F.; Lei, S.; Woods, J.; Rose, J.; Marshall, D. D.; Riekeberg, E.; De Lima Leite, A.; Morton, M.; Dodds, E. D.; Franco, R.; et al. Metabolomics Analyses from Tissues in Parkinson's Disease. *Methods Mol. Biol.* **2019**, *1996*, 217−257.
(94) Bhinderwala, F.; Powers, R. NMR Metabolomics Protocols for Drug Discovery. *Methods Mol. Biol.* **2019**, *2037*, 265−311.

https://doi.org/10.1021/acschemneuro.3c00678
ACS Chem. Neurosci. 2024, 15, 1110−1124